Gust Rejection Properties of VTOL Multirotor Aircraft*

James F. Whidborne, Alastair K. Cooke

Centre for Aeronautics, Cranfield University, Bedfordshire, United Kingdom.

December 2017

Abstract

The effect of rotor aerodynamics on the stability and control of multi-rotor aircraft is explored by analysis of a conceptual planar birotor aircraft. In particular, the effect of rotor tilt on the stability and zero-location is investigated. Furthermore, it is shown that designing the vehicle with outwards rotor tilt potentially results in dramatic improvement in the gust rejection properties of the vehicle.

1 Introduction

The use and application of quadrotor and other multirotor unmanned aircraft (popularly known as drones) has proliferated over the last few years. Probably the most common application is for aerial photography, whilst surveillance is also a much suggested use. For both of these, stable hovering is an important requirement. Hence it is important that the aircraft is resistant to transient winds and gusts, particularly for operation in urban areas where there is a likelihood of collisions with buildings.

Aerodynamic modelling and analysis of traditional rotorcraft is well-established; classic texts include Bramwell [1976], Seddon [1990], Leishman [2000]. There has been some work to analyze the aerodynamics of multirotor vehicles or to include the aerodynamics in control system models. The aerodynamic modelling of the rotor aerodynamics is usually based on the established methods for rotorcraft, see Pounds et al. [2004] for example. Early experimental work, supported by analytical modelling, was undertaken by Martínez [2007]. Analytical aerodynamic modelling was performed by Waslander and Wang [2009] and the effects of horizontal wind and gusting analyzed, and a control scheme to ameliorate the effects was proposed. Similar models were used to analyze the control in aggressive manoeuvring by Huang et al. [2009]. Another noted work is by Bristeau et al. [2009], where the effect of the centre of gravity location on the stability and the lateral gust rejection was analyzed. Other quadrotor work that includes aerodynamic modelling includes Naidoo et al. [2011], Sydney et al. [2013] and Kai et al. [2017], while Del Cont Bernard et al. [2017] have studied ground effect.

What distinguishes the work presented here is that an analysis of the rotor tilt is performed. Usually, the thrust on quadrotors is assumed to act in parallel with the body frame z-axis. In practice, there is often a small inward tilt towards the z-axis resulting from the loading of the airframe. As we will see, this small tilt aids stability, and is hence safely ignored in the modelling. However, like the centre of gravity location, the degree of rotor tilt affects the stability and gust rejection properties as we will show. In order to simplify the analysis, a conceptual vehicle, a birotor that is constrained to operate in a vertical plain, is modelled. This simplifies the analysis and makes it easier to understand the trade-offs. The paper starts with a brief description of rotor aerodynamic modelling. A steady state analysis of the rotor aerodynamic properties is performed. This is followed in Section 3 by a presentation of the equations of motion for the planar birotor that includes the tilt angle. Trim conditions are presented. In Section 4, an analysis of the dynamics including the tilt but excluding the aerodynamics is first performed to establish the non-minimum phase behaviour. The full model is then linearized and the dependence of the stability on the tilt angle is analyzed. In Section 5, the gust rejection properties of the vehicle are investigated. A stabilizing LQR controller is designed, and through simulation of the nonlinear controlled system, it is found that although an outward tilt gives a statically unstable system, with stabilizing feedback a significant ability to counter horizontal gusts is produced. The paper concludes with some discussion and suggestions for further work.

---

2 Rotor Aerodynamic Modelling

Consider a rotor disc in a horizontal airflow as shown in Figure 1. The thrust of a rotor in the axial direction, T, is given by

$$T = \rho A (\Omega R)^2 C_T \tag{1}$$

where ρ is the air density, A is the rotor disc area, Ω is the rotor angular velocity, R is the rotor radius and C_T is the rotor thrust coefficient. Similarly, the in-plane horizontal drag force, H, is given by

$$H = \rho A (\Omega R)^2 C_H \tag{2}$$

where C_H is the drag coefficient. For a rotor with hinged blades, there is an insignificant moment caused by the air flow. Most small multirotor vehicles use unhinged blades, which means this moment may be significant, but for the purpose of this study we will assume it is not.
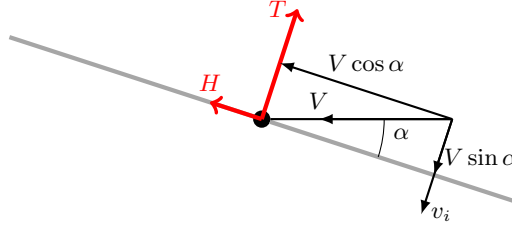

Figure 1: Disc incidence and component velocities in an airflow [Seddon, 1990, p. 56]

2.1 Thrust Coefficient

Based on the original work of Glauert, the thrust coefficient can be determined from momentum theory. If the flapping term is ignored, the following expression can be derived [Seddon, 1990, p. 59] (also see Bramwell [1976, p. 147]).

$$C_T = \tfrac{1}{2}\sigma a \left[\tfrac{1}{3}\theta \left(1 + \tfrac{3}{2}\mu^2 \right) - \tfrac{1}{2}\lambda \right] \tag{3}$$

where σ is the solidity factor, a is the lift slope of the blade, θ is the rotor blade pitch angle, μ is the advance ratio, also being the lateral wind component and λ is the inflow ratio. The solidity factor for a rotor with radius R and b blades of constant chord, c, is defined as $\sigma = bc/(\pi R)$ [Bramwell, 1976, p. 91]. For a tapering blade, the chord is taken as that at 3/4 radius [Bramwell, 1976, p. 147]. Similarly for blades with a linear twist, the equation is still valid provided the the pitch angle at 3/4 radius is used [Bramwell, 1976, p. 147]. The advance ratio is [Seddon, 1990, p. 56]

$$\mu = \frac{V \cos \alpha}{\Omega R} \tag{4}$$

where V is the incident flow speed and α is the angle between the incident flow and the tip-path plane as shown in Figure 1.

The inflow ratio is given by [Seddon, 1990, p. 56]

$$\lambda = \frac{V \sin \alpha + v_i}{\Omega R} \tag{5}$$

where v_i is the induced velocity. By assuming the induced velocity is constant over the whole disc, using momentum theory the induced velocity can be calculated from [Seddon, 1990, p. 52]

$$\left(\frac{v_i}{v_h} \right)^4 + \left(\frac{V}{v_h} \right)^2 \left(\frac{v_i}{v_h} \right)^2 = 1 \tag{6}$$

where v_h is the induced velocity in hover at the same thrust which is calculated from

$$v_h^2 = \frac{T}{2\rho A}. \tag{7}$$

2.2 Blade Profile Drag Coefficient

When the rotor is subjected to a lateral air speed, there is a resulting in-plane horizontal drag force, consisting mainly of the blade profile drag. From Bramwell [1976, p. 149], the drag coefficient is given by

$$C_H = \frac{a\sigma}{2}\left[\frac{\mu\delta}{2a} + \frac{1}{3}a_1\theta_0 + \frac{3}{4}\lambda a_1 - \frac{1}{2}\mu\theta_0\lambda + \frac{1}{4}\mu a_1^2\right] \tag{8}$$

where δ is the blade profile drag coefficient and a_1 is the backward flapping angle which can be calculated from [Seddon, 1990, p. 65, eq. (5.50)]

$$a_1 = \frac{\mu(8\theta_0/3 - 2\lambda)}{1 - \mu^2/2}. \tag{9}$$

2.3 Thrust and Drag Mappings

Force and moment control is effected on the vehicle by adjusting the thrust of each rotor by varying Ω by means of a speed servocontroller. Thus in order to design the controller and to analyze the dynamics, we require the mappings from Ω to the pair (T, H). However, the thrust, drag pair is also dependent upon the airspeed, V, and the airspeed incidence angle, α. Hence we require the mappings from the triple (Ω, α, V), onto (T, H).

The equations describing the mapping $(\Omega, \alpha, V) \mapsto (T, H)$ are given by (1) – (9). However, the appearance of T in (7) means the equations are implicit and an explicit solution appears intractable. Hence calculation of the mapping requires a numerical method, here we have used the MATLAB routine, `fzero`.
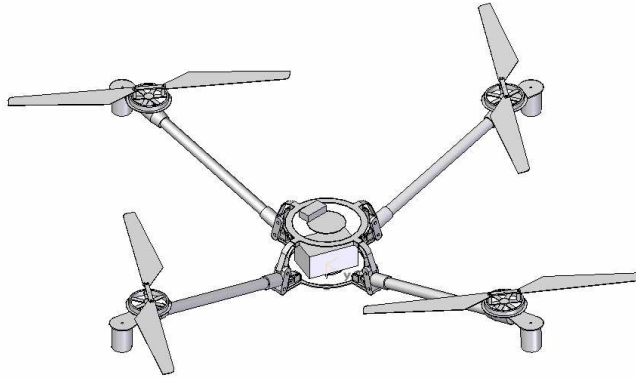

Figure 2: Draganflyer X-Pro quadrotor [Martínez, 2007]

As an example, we use the rotors for the Draganflyer X-Pro quadrotor shown in Figure 2 for which the relevant parameters have been obtained by windtunnel and other experiments [Martínez, 2007] and are given by $a = 5.5$, $R = 0.258$ m, $c = 0.04$ m, $b = 2$, $\theta_0 = 0.3025$ rad and $\delta = 0.05$. The mapping for $(\Omega, \alpha) \mapsto T$ for constant airspeed values $V = \{0, 5, 10\}$ m/s, is shown in Figure 3.

3 Equations of Motion

Now let us apply the thrust to a conceptual vehicle, a 2-rotor VTOL vehicle that operates only on the vertical (x, y)-plane as shown in Figure 4 where the rotors are symmetrically tilted with an angle Γ. The weight of the vehicle is W, ϕ is the pitch/roll angle, V_w is the wind which is assumed to be horizontal, $T_i(\Omega_i, \alpha_i, V_i)$, and $H_i(\Omega_i, \alpha_i, V_i)$, $i = 1, 2$ are the thrusts and drags respectively of the ith rotor. Since we are interested in the gust rejection properties, the inertial frame is taken as the frame of reference. So from Figure 4 and dropping the notation of dependence of T_i,
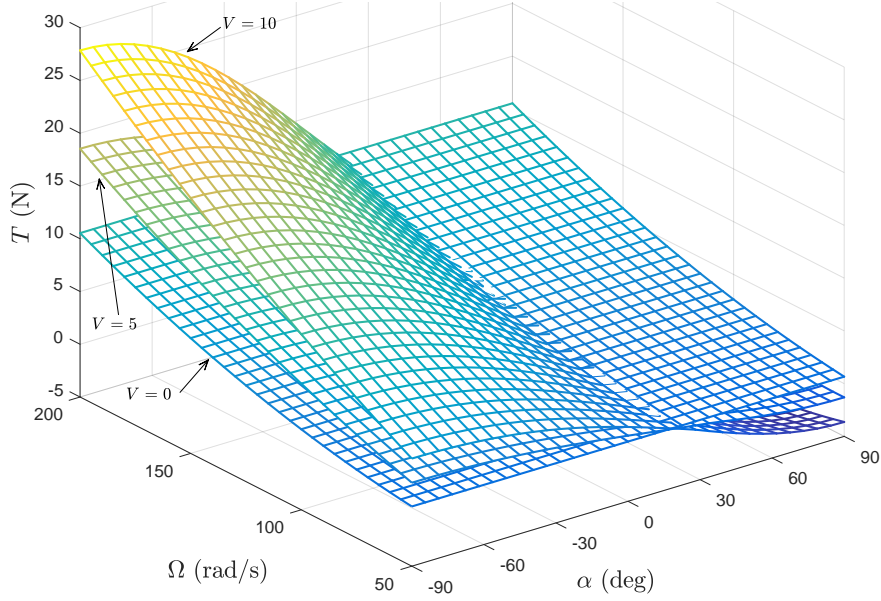
Figure 3: Thrust mapping for airspeeds $V = \{0, 5, 10\}$.

H_i on $(\Omega_i, \alpha_i, V_i)$, the equations of motion for the vehicle are

$$m\ddot{y} = T_1\, \mathrm{c}(\phi + \Gamma) + T_2\, \mathrm{c}(\phi - \Gamma) - H_1\, \mathrm{s}(\phi + \Gamma) - H_2\, \mathrm{s}(\phi - \Gamma) - W \tag{10}$$

$$m\ddot{x} = -T_1\, \mathrm{s}(\phi + \Gamma) - T_2\, \mathrm{s}(\phi - \Gamma) - H_1\, \mathrm{c}(\phi + \Gamma) - H_2\, \mathrm{c}(\phi - \Gamma) \tag{11}$$

$$I\ddot{\phi} = (T_1 - T_2)\, \ell\, \mathrm{c}\,\Gamma - (H_1 + H_2)\, \ell\, \mathrm{s}\,\Gamma \tag{12}$$

$$\alpha_1 = \arctan\left((\dot{y} + \ell\dot{\phi}\, \mathrm{c}\,\phi)/(V_w + \dot{x} - \ell\dot{\phi}\, \mathrm{s}\,\phi) \right) - \phi - \Gamma \tag{13}$$

$$\alpha_2 = \arctan\left((\dot{y} - \ell\dot{\phi}\, \mathrm{c}\,\phi)/(V_w + \dot{x} + \ell\dot{\phi}\, \mathrm{s}\,\phi) \right) - \phi + \Gamma \tag{14}$$

$$V_1 = \sqrt{\left(\dot{y} + \ell\dot{\phi}\, \mathrm{c}\,\phi\right)^2 + \left(V_w + \dot{x} - \ell\dot{\phi}\, \mathrm{s}\,\phi\right)^2} \tag{15}$$

$$V_2 = \sqrt{\left(\dot{y} - \ell\dot{\phi}\, \mathrm{c}\,\phi\right)^2 + \left(V_w + \dot{x} + \ell\dot{\phi}\, \mathrm{s}\,\phi\right)^2} \tag{16}$$

where $\mathrm{s}(\cdot)$ denotes $\sin(\cdot)$, $\mathrm{c}(\cdot)$ denotes $\cos(\cdot)$ and where I is the moment of inertia, m is mass, ℓ is the arm-length and $W = mg$ where g is the gravitational constant.

Rearranging (10), (11) and (12) gives

$$m\ddot{y} = (T_1 + T_2)\, \mathrm{c}\,\phi\, \mathrm{c}\,\Gamma - (T_1 - T_2)\, \mathrm{s}\,\phi\, \mathrm{s}\,\Gamma - (H_1 + H_2)\, \mathrm{s}\,\phi\, \mathrm{c}\,\Gamma - (H_1 - H_2)\, \mathrm{c}\,\phi\, \mathrm{s}\,\Gamma - W, \tag{17}$$

$$m\ddot{x} = -(T_1 + T_2)\, \mathrm{s}\,\phi\, \mathrm{c}\,\Gamma - (T_1 - T_2)\, \mathrm{c}\,\phi\, \mathrm{s}\,\Gamma - (H_1 + H_2)\, \mathrm{c}\,\phi\, \mathrm{c}\,\Gamma + (H_1 - H_2)\, \mathrm{s}\,\phi\, \mathrm{s}\,\Gamma, \tag{18}$$

$$I\ddot{\phi} = (T_1 - T_2)\ell\, \mathrm{c}\,\Gamma - (H_1 + H_2)\ell\, \mathrm{s}\,\Gamma. \tag{19}$$

With the vehicle in moving air but trimmed at hover in the earth coordinates, the trimmed variables are the roll angle and the rotor speeds denoted by $\hat{\phi}$ and $\hat{\Omega}_i$, $i = 1, 2$ respectively. Setting the rates and accelerations to zero gives, from (17) – (19),

$$(T_1 + T_2)\, \mathrm{c}\,\phi\, \mathrm{c}\,\Gamma - (T_1 - T_2)\, \mathrm{s}\,\phi\, \mathrm{s}\,\Gamma = W + (H_1 + H_2)\, \mathrm{s}\,\phi\, \mathrm{c}\,\Gamma + (H_1 - H_2)\, \mathrm{c}\,\phi\, \mathrm{s}\,\Gamma \tag{20}$$

$$(T_1 + T_2)\, \mathrm{s}\,\phi\, \mathrm{c}\,\Gamma + (T_1 - T_2)\, \mathrm{c}\,\phi\, \mathrm{s}\,\Gamma = -(H_1 + H_2)\, \mathrm{c}\,\phi\, \mathrm{c}\,\Gamma - (H_1 - H_2)\, \mathrm{s}\,\phi\, \mathrm{s}\,\Gamma \tag{21}$$

$$(T_1 - T_2)\ell\, \mathrm{c}\,\Gamma = (H_1 + H_2)\ell\, \mathrm{s}\,\Gamma \tag{22}$$

Now, T_i and H_i are dependent upon the rotor speed, Ω_i, but the implicit nature of the thrust mapping makes an explicit solution intractable. Hence we must use a numerical method for trimming the vehicle. Note that in still air, with $V = 0$, the solution is obtained trivially as $\hat{\phi} = 0$ and $\hat{T} = W/(2\cos\Gamma)$.

Using the geometry based on the Draganflyer X-Pro quadrotor, we assume $I = 0.0625$ kg m^2, $m = 2.36/2$ kg, $\ell = 0.45$ m and $\Gamma = 0$ [Martínez, 2007]. The trim is calculated using (20) – (22) and using the MATLAB routine,
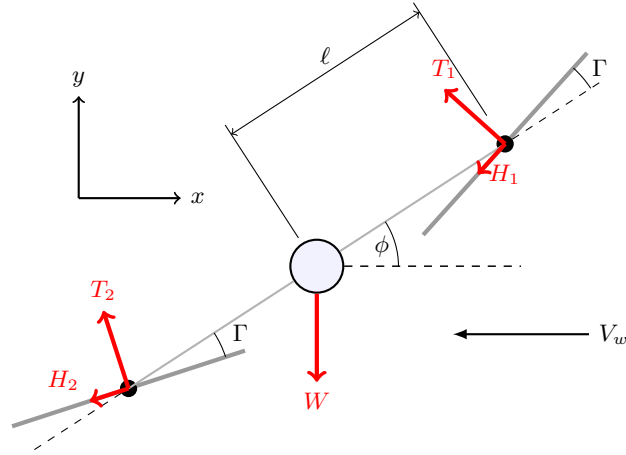
4

Figure 4: Planar VTOL vehicle schematic

`fminsearch` to minimize the residual. The result for $V_w \in [0, 20]$ m/s is shown in Figure 5. For low horizontal windspeeds, the trim rotor speed actually decreases. This appears counter-intuitive, but is due to the lift that the wind provides.
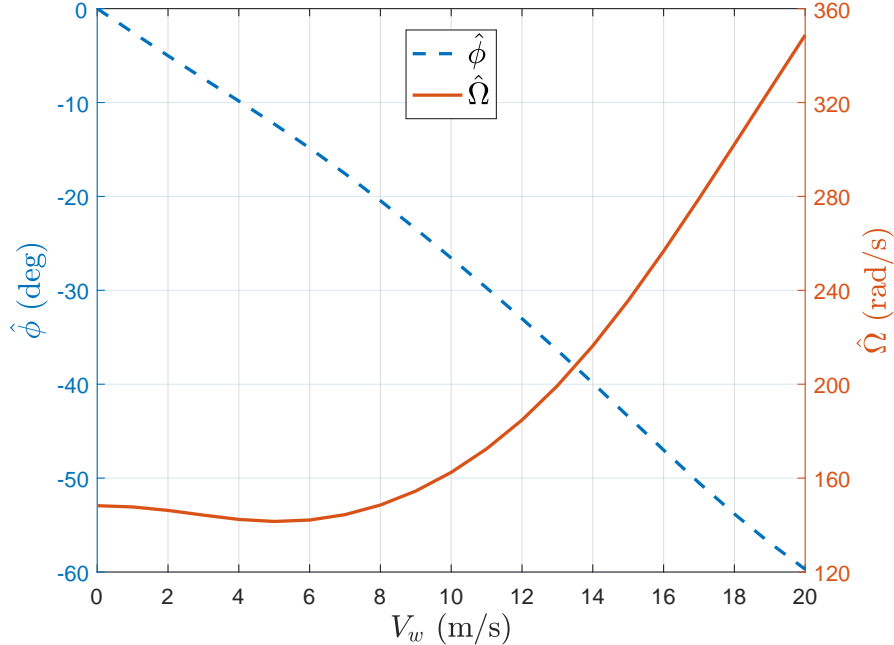

Figure 5: Variation in trim for $V_w \in [0, 20]$ m/s with $\Gamma = 0$.

4   Linear Analysis

4.1   Ignoring the Rotor Aerodynamics

Let us start by analyzing the effect of the rotor tilt angle, Γ on a linearized model of the dynamics in still air ignoring the aerodynamics of the rotor. From $(11) - (12)$, defining the state as

$$\mathbf{x} = \begin{bmatrix} \dot{y}, & y, & \dot{x}, & x, & \dot{\phi}, & \phi - \hat{\phi} \end{bmatrix}^T. \tag{23}$$

The rotor aerodynamics are ignored, so the control is effected purely by the thrusts, T_i, and the horizontal components, H_i, are assumed to be zero. Hence

$$\mathbf{u}_T = \begin{bmatrix} (T_1 + T_2) - 2\hat{T}, & (T_1 - T_2) \end{bmatrix}^T \tag{24}$$

5

and assuming small perturbations about trim, the small perturbation linear model is given by

$$\dot{\mathbf{x}} = \mathbf{A}_T\mathbf{x} + \mathbf{B}_T\mathbf{u}_T \tag{25}$$

where

$$\mathbf{A}_T = \begin{bmatrix} 0 & 1 & 0 & 0 & 0 & 0 \\ 0 & 0 & 0 & 0 & -2\hat{T}\sin\hat{\phi}\cos\Gamma/m & 0 \\ 0 & 0 & 0 & 1 & 0 & 0 \\ 0 & 0 & 0 & 0 & -2\hat{T}\cos\hat{\phi}\cos\Gamma/m & 0 \\ 0 & 0 & 0 & 0 & 0 & 1 \\ 0 & 0 & 0 & 0 & 0 & 0 \end{bmatrix}, \tag{26}$$

$$\mathbf{B}_T = \begin{bmatrix} 0 & 0 \\ \cos\hat{\phi}\cos\Gamma/m & -\sin\hat{\phi}\sin\Gamma/m \\ 0 & 0 \\ -\sin\hat{\phi}\cos\Gamma/m & -\cos\hat{\phi}\sin\Gamma/m \\ 0 & 0 \\ 0 & \ell\cos\Gamma/I \end{bmatrix}. \tag{27}$$

Substituting the trim values $\hat{T} = mg/(2\cos\Gamma)$ and $\hat{\phi} = 0$ we get

$$\mathbf{A}_T = \begin{bmatrix} 0 & 1 & 0 & 0 & 0 & 0 \\ 0 & 0 & 0 & 0 & 0 & 0 \\ 0 & 0 & 0 & 1 & 0 & 0 \\ 0 & 0 & 0 & 0 & -g & 0 \\ 0 & 0 & 0 & 0 & 0 & 1 \\ 0 & 0 & 0 & 0 & 0 & 0 \end{bmatrix}, \qquad \mathbf{B}_T = \begin{bmatrix} 0 & 0 \\ \cos\Gamma/m & 0 \\ 0 & 0 \\ 0 & -\sin\Gamma/m \\ 0 & 0 \\ 0 & \ell\cos\Gamma/I \end{bmatrix}. \tag{28}$$

The system transfer function matrix with output $\mathbf{y} = \begin{bmatrix} y, & x, & \phi \end{bmatrix}^T$ is given by

$$G_T = \begin{bmatrix} \cos\Gamma/(ms) & 0 \\ 0 & -(I\sin\Gamma s^2 + mg\ell\cos\Gamma)/(mIs^3) \\ 0 & \ell\cos\Gamma/(Is) \end{bmatrix}. \tag{29}$$

Thus there is a pair of zeros in the lateral position channel located at $s = \sqrt{-mg\ell/(I\tan\Gamma)}$. If Γ is small, then the zeros are high frequency and have little impact on the closed loop system performance. If $\Gamma < 0$, there is a nonminimum phase zero. Significantly, $\mathbf{A}_T$ is independent of Γ, so open-loop stability is invariant, but $\mathbf{B}_T$ is dependent on Γ, and some direct control of the lateral position rate is achieved for $\Gamma \neq 0$, but this is adverse for $\Gamma < 0$, which causes the nonminimum phase zero.

4.2 Including Rotor Aerodynamics

We now extend the model to that given by (10) – (16) with the aerodynamic effects included. Thus T_i, H_i, are dependent upon the state, $\mathbf{x}$, control, $\mathbf{u}_\Omega$ and wind disturbance V_w, where the control is

$$\mathbf{u}_\Omega = \begin{bmatrix} \Omega_1 + \Omega_2 - \hat{\Omega}_1 - \hat{\Omega}_2, & \Omega_1 - \Omega_2 + \hat{\Omega}_1 - \hat{\Omega}_2 \end{bmatrix}^T. \tag{30}$$

The dynamic equations, (10) – (16) , are linearized at a set of trim points using second order finite difference method to provide a small perturbation model

$$\dot{\mathbf{x}} = \mathbf{A}\mathbf{x} + \mathbf{B}_\Omega\mathbf{u}_\Omega + \mathbf{B}_w u_w. \tag{31}$$

that includes the external disturbance given by $u_w = V_w - \hat{V}_w$.

With $\hat{V}_w = 0$, inclusion of the aerodynamics model has introduced negative aerodynamic derivative damping terms $Y_v = \partial\dot{u}/\partial u$, $X_u = \partial\dot{v}/\partial v$ and $N_\omega = \partial\dot{\omega}/\partial\omega$ into the linearized system matrix $\mathbf{A}$ that are absent from $\mathbf{A}_T$ in (28). The matrix $\mathbf{A}$ is denoted by

$$\mathbf{A} = \begin{bmatrix} 0 & 1 & 0 & 0 & 0 & 0 \\ 0 & Y_v & 0 & 0 & 0 & 0 \\ 0 & 0 & 0 & 1 & 0 & 0 \\ 0 & 0 & 0 & X_u & -g & X_\omega \\ 0 & 0 & 0 & 0 & 0 & 1 \\ 0 & 0 & 0 & N_u & 0 & N_\omega \end{bmatrix} \tag{32}$$

6

and the further two terms, N_u and N_ω, are cross-coupling aerodynamic derivatives, the remaining aerodynamic derivatives are all nearly zero. Figure 6 shows the variation of $\{Y_v, X_u, X_\omega, N_u, N_\omega\}$ with Γ. Note that for $\Gamma = 0$, $X_\omega = N_u = 0$ and the resulting eigenvalues are $\{N_w, X_u, Y_v, 0, 0, 0\}$.
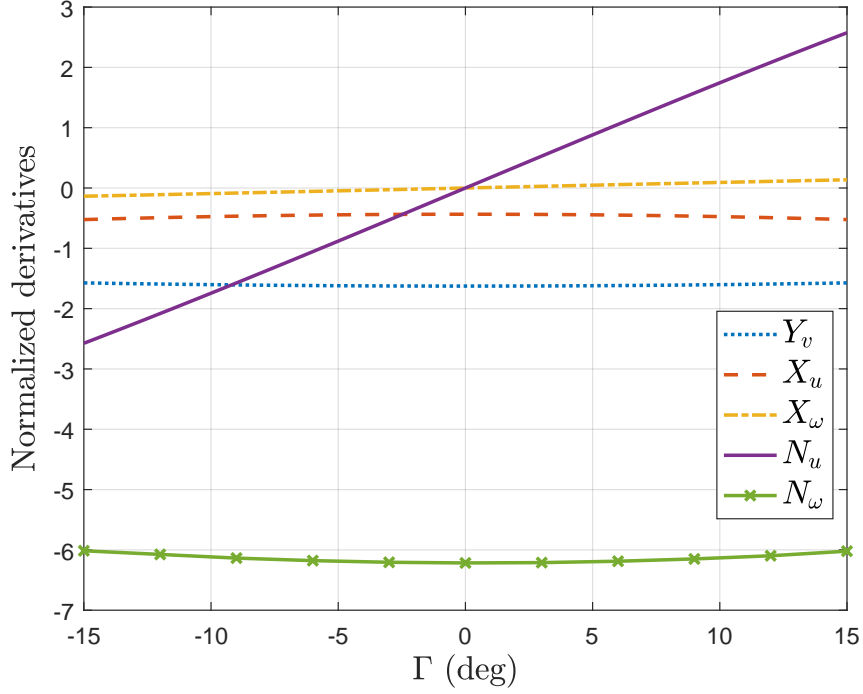

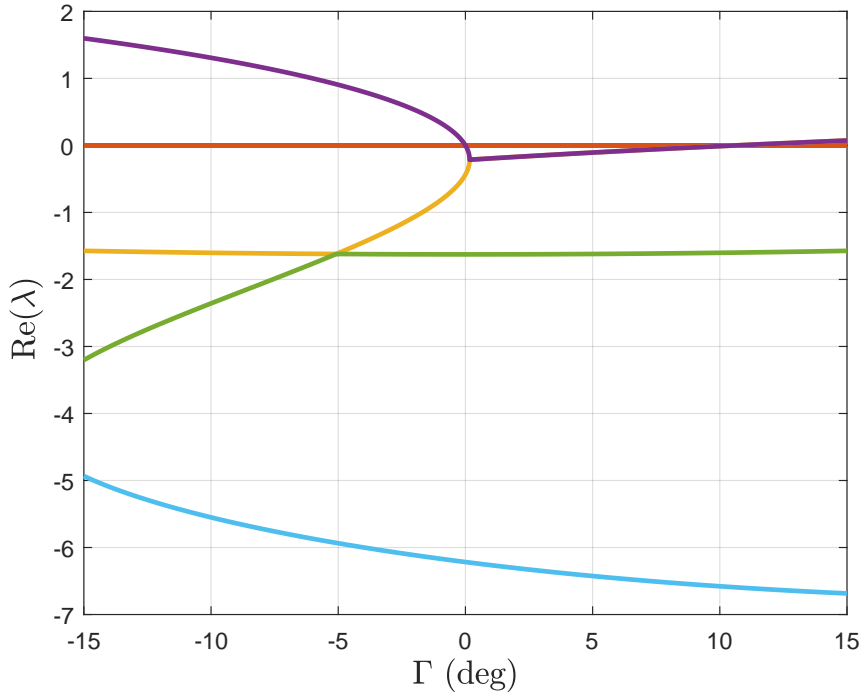Figure 6: Variation of aerodynamic derivatives, $\{Y_v, X_u, X_\omega, N_u, N_\omega\}$, with Γ for $V_w = 0$.

Figure 7: Variation in real parts of eigenvalues of small perturbation model for $V_w = 0$.

The resulting characteristic equation is

$$Q(\lambda) = \lambda^2 (\lambda - Y_v) \left(\lambda^3 - (N_w + X_u)\lambda^2 + (N_\omega X_u - N_u X_\omega)\lambda + N_u g \right) \tag{33}$$

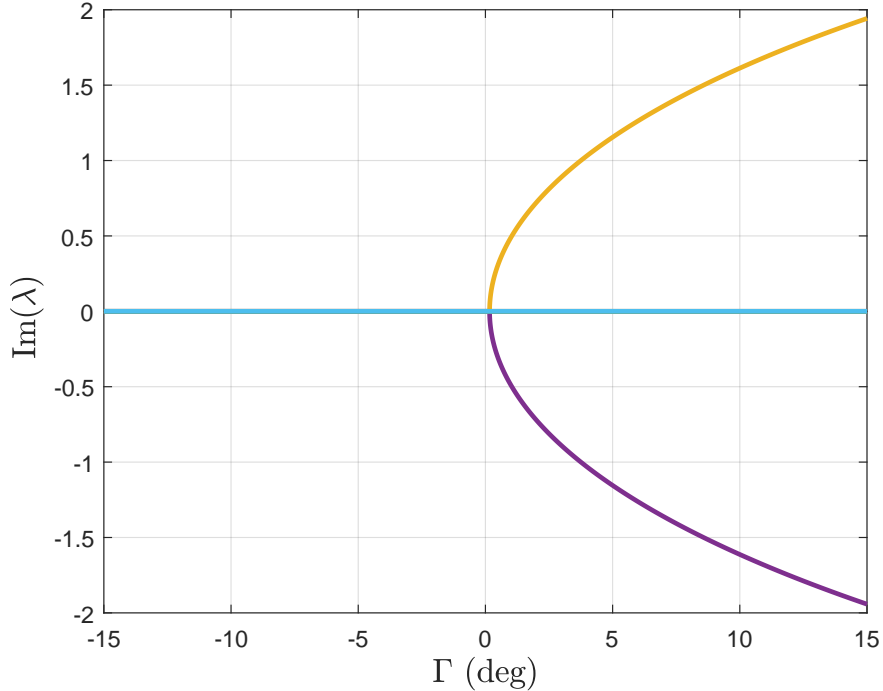Figures 7 and 8 show the dependence of the real and imaginary parts respectively of the eigenvalues on Γ. Note

Figure 8: Variation in imaginary parts of eigenvalues of small perturbation model for $V_w = 0$.

the high eigenvalue sensitivity when Γ is near zero. It is easily shown from the Routh-Hurwitz criterion that for $\Gamma < 0$, the negative values of the $N_u g$ term in (33) causes the instability. For $\Gamma > 0$ stability is also lost when $N_u g > (N_u X_\omega - N_\omega X_u)(N_\omega + X_u)$, which occurs for $\Gamma \simeq 10.62°$.

However, inspection of $\mathbf{B}_w$ shows the sensitivity of the pitch rotation rate to the wind disturbance, V_w. Letting

$$\mathbf{B}_w = \begin{bmatrix} 0 & Y_{V_w} & 0 & X_{V_w} & 0 & N_{V_w} \end{bmatrix}^T,\tag{34}$$

the variation in disturbance derivatives, $\{N_{V_w}, X_{V_w}, Y_{V_w}\}$ is shown in Figure 9. We see that, although $\Gamma < 0$ causes instability, it also provides a moment that causes the vehicle to tilt into the wind when subjected to a lateral gust. This is potentially beneficial for gust rejection. This property is explored in the next section.

5   Linear control

In order to investigate the gust rejection properties of a vehicle with negative Γ, a stabilizing controller is designed. Good control of quadrotors for non-aggressive manoeuvring near hover can be easily obtained using LQR control [Cowling et al., 2006, 2010, for example].

The LQR control problem is very well known. For a linear state-space model of the plants dynamics

$$\dot{\mathbf{x}}(t) = \mathbf{A}\mathbf{x}(t) + \mathbf{B}\mathbf{u}(t),\tag{35}$$

a control input $\mathbf{u}(t) = -K_c\mathbf{x}(t)$ is determined such that the closed loop system $\dot{\mathbf{x}} = [A - BK_c]\mathbf{x}(t)$ is stable and a gain K_c can be determined that minimizes the performance measure, J, where

$$J = \int_0^\infty \left(\mathbf{x}(t)Q\mathbf{x}(t) + \mathbf{u}(t)R\mathbf{u}(t) \right)\ \mathbf{t}\tag{36}$$

and Q and R are weighting matrices.

The gust rejection effectiveness is tested by means of simulation of the nonlinear plant model (18) – (19) with an LQR controller synthesized using the MATLAB `lqr` routine with $Q = \mathrm{diag} \begin{bmatrix} 100 & 1 & 1 & 1 & 1 & 1 \end{bmatrix}$ and $R = \mathrm{diag} \begin{bmatrix} 1/2 & 1/2 \end{bmatrix}$. Four sets of results are presented for $\Gamma = \{-10°, -5°, 0°, 5°\}$. The lateral position, x, and roll angle, ϕ, responses to a lateral position step demand of 5 m are presented in Figures 10 and 11 respectively. These show marginally better performance for greater Γ. This is expected because of the introduction of the non-minimum
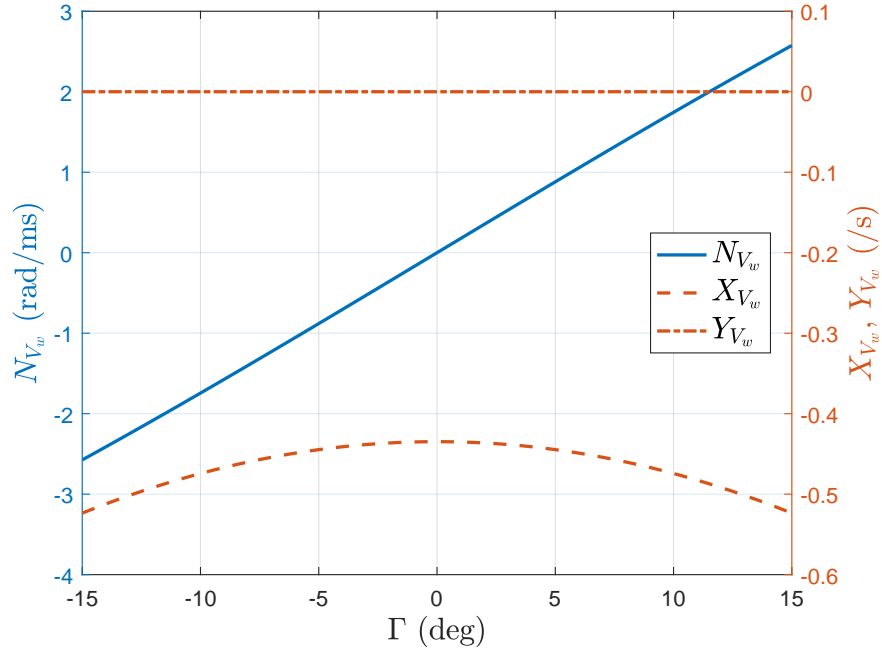
Figure 9: Variation in disturbance derivatives $\{N_{V_w}, X_{V_w}, Y_{V_w}\}$ with Γ for $V_w = 0$.
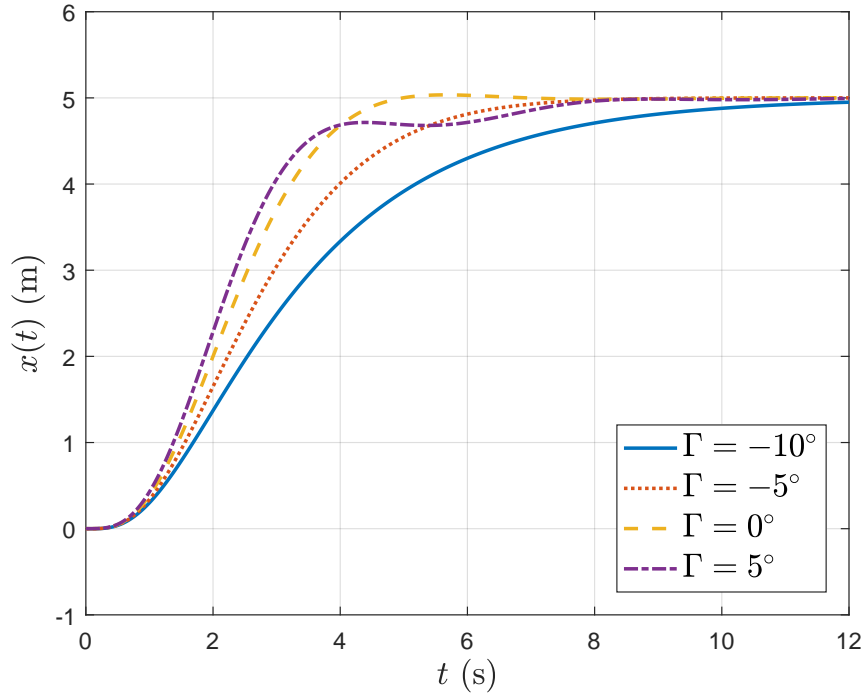

Figure 10: Lateral position response to 5 m lateral position step demand.

phase zero and pole for $\Gamma < 0$ as discussed in the preceding section. There is a small amount of initial undershoot in the step response of x for $\Gamma < 0$, but it is barely perceptible in Figures 10.

Responses of lateral position and the roll angle to a lateral wind velocity step of 5 m/s are presented in Figures 12 and 13. The gust rejection properties of the vehicle with $\Gamma < 0$ are remarkable, for $\Gamma = -10°$, the vehicle actually pitches into the wind so much that the lateral position error is negative, meaning that the vehicle actually moves up-wind. It must be remembered though, that the vehicle body drag has been ignored, and this would reduce the effect. For $\Gamma = 5°$, the effect of the gust on the lateral position is severe, resulting in an 8 m displacement. Note that the controller does not contain integral action, so the controller does not compensate for this lateral error.
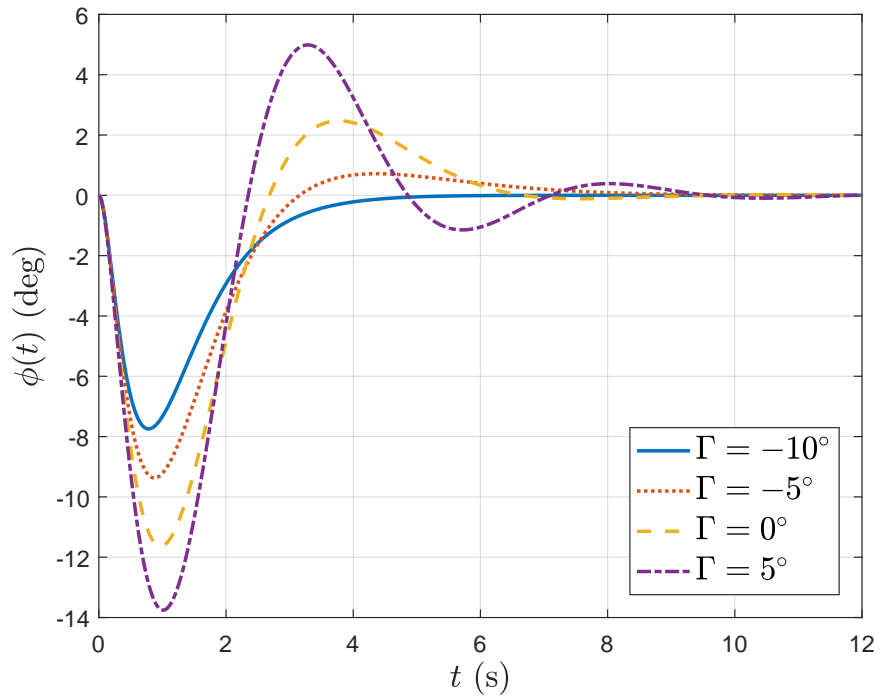
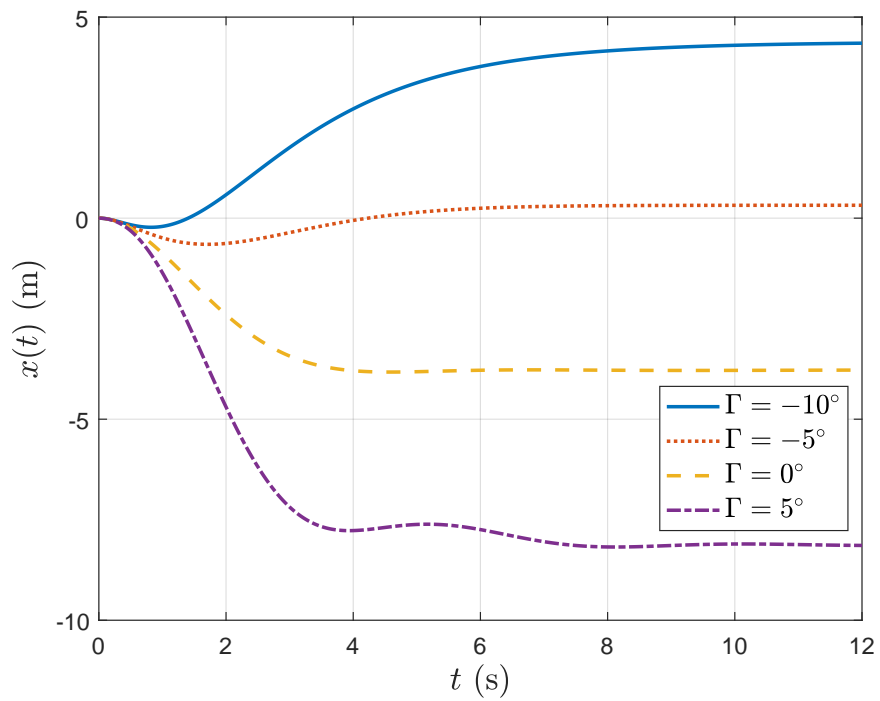Figure 11: Roll angle response to 5 m lateral position step demand.

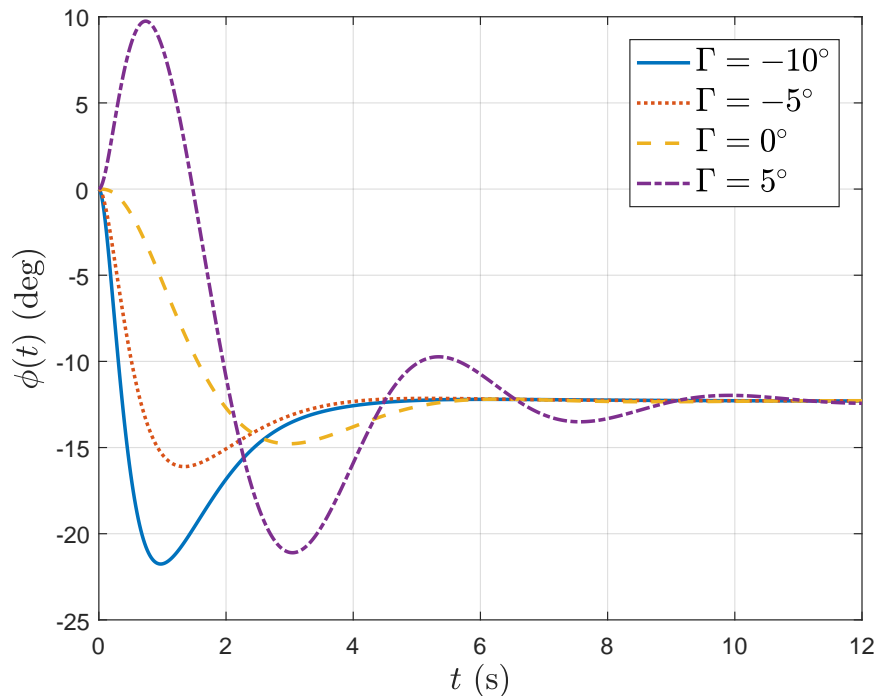Figure 12: Lateral position response to 5 m/s horizontal wind speed step.

Figure 13: Roll angle response to 5 m/s horizontal wind speed step.

6 Conclusions

The paper investigates some of the effects of the rotor aerodynamics on the control of a conceptual birotor VTOL aircraft. The analysis can be extended to quadrotor and other multirotor aircraft. The main finding is the effect of including tilt on the rotors. A positive tilt (inwards) results in increased open-loop static stability, although dynamic stability can be lost for large tilt. A negative tilt (outwards) results in a loss of static stability and some non-minimum phase. For small tilt angles, the non-minimum phase behaviour is high frequency and appears to have little effect on the control performance. However, the gust rejection properties are dramatically improved with negative tilt. Effectively, this introduces anhedral into the aircraft; the gust disturbance rejection properties of anhedral in fixed wing aircraft are fairly well-known, and is the reason why VTOL fixed wing aircraft such as the Harrier have notable anhedral. The dynamics of such aircraft are extensively explored in Hauser et al. [1992].

The aerodynamic properties of the quadrotor vehicle on which the conceptual birotor of this study is based, namely the Draganflyer X-Pro quadrotor, have been investigated experimentally [Martínez, 2007]. It remains for further work to extend this study to a quadrotor and to validate the findings based on the results of Martínez [2007]. Furthermore, by making some simplifying assumptions to the aerodynamic and equations of motion, a detailed study of the nonlinear dynamics in a similar manner to Hauser et al. [1992] could be conducted. Experimental validation is an obvious further step.

References

A. R. S. Bramwell. *Helicopter Dynamics*. Edward Arnold, London, U.K., 1976.

P. J. Bristeau, P. Martin, E. Salaün, and N. Petit. The role of propeller aerodynamics in the model of a quadrotor UAV. In *2009 European Control Conference (ECC)*, pages 683–688, Budapest, Hungary, Aug 2009.

I. D. Cowling, J. F. Whidborne, and A. K. Cooke. Optimal trajectory planning and LQR control for a quadrotor UAV. In *Proc. UKACC Int. Conf. Control 2006 (ICC2006)*, page CD ROM paper 125, Glasgow, UK, Sept. 2006.

I. D. Cowling, O. A. Yakimenko, J. F. Whidborne, and A. K. Cooke. Direct method based control system for an autonomous quadrotor. *J. Intell. Robotic Syst.*, 60(2):285 –316, 2010. doi: 10.1007/s10846-010-9416-9.

D. Del Cont Bernard, F. Riccardi, M. Giurato, and M. Lovera. A dynamic analysis of ground effect for a quadrotor platform. In *Proc. 20th IFAC World Congress*, Toulouse, France, July 2017.

J. Hauser, S. Sastry, and G. Meyer. Nonlinear control design for slightly non-minimum phase systems: Application to V/STOL aircraft. *Automatica*, 28(4):665–679, 1992. ISSN 0005-1098. doi: 10.1016/0005-1098(92)90029-F.

H. Huang, G. M. Hoffmann, S. L. Waslander, and C. J. Tomlin. Aerodynamics and control of autonomous quadrotor helicopters in aggressive maneuvering. In *Proc. 2009 IEEE International Conference on Robotics and Automation*, pages 3277–3282, May 2009. doi: 10.1109/ROBOT.2009.5152561.

J.-M. Kai, G. Allibert, M.-D. Hua, and T. Hamel. Nonlinear feedback control of quadrotors exploiting first-order drag effects. In *Proc. 20th IFAC World Congress*, Toulouse, France, July 2017.

J. G. Leishman. *Principles of Helicopter Aerodynamics*. Cambridge University Press, Cambridge, U.K., 2000.

V. M. Martínez. Modelling of the flight dynamics of a quadrotor helicopter. MSc dissertation, Cranfield University, Bedfordshire, U.K., 2007.

Y. Naidoo, R. Stopforth, and G. Bright. Rotor aerodynamic analysis of a quadrotor for thrust critical applications. In *4th Robotics and Mechatronics Conference of South Africa (ROBMECH 2011)*, Pretoria, South Africa, Nov. 2011.

P. Pounds, R. Mahoney, J. Gresham, P. Corke, and J. Roberts. Towards dynamically favourable quad-rotor aerial robots. In *Proc. Austr. Conf. Robo. Auto.*, Canberra, Australia, 2004.

J. Seddon. *Basic Helicopter Aerodynamics*. BSP Professional, Oxford, U.K., 1990.

N. Sydney, B. Smyth, and D. A. Paley. Dynamic control of autonomous quadrotor flight in an estimated wind field. In *52nd IEEE Conference on Decision and Control (CDC)*, pages 3609–3616, Florence, Italy, Dec. 2013. doi: 10.1109/CDC.2013.6760438.

S. Waslander and C. Wang. Wind disturbance estimation and rejection for quadrotor position control. In *AIAA Infotech@Aerospace Conferences*, number AIAA 2009-1983, Seattle, WA, Apr. 2009. doi: 10.2514/6.2009-1983.